Probing Src Homology 2 Domain Ligand Interactions by Differential Line Broadening†

Ulrich Günther,*,‡ Tanja Mittag,‡ and Brian Schaffhausen§

Institute of Biophysical Chemistry, J. W. Goethe University, Frankfurt, Biocenter N230, Marie-Curie-Strasse 9, 60439 Frankfurt, Germany, and Department of Biochemistry, School of Medicine, Tufts University, 136 Harrison Avenue, Boston, Massachusetts 02111

Received March 29, 2002; Revised Manuscript Received July 18, 2002

ABSTRACT: Few techniques for probing the role of individual amino acids in interactions of a protein with ligands are available. Chemical shift perturbations in NMR spectra provide qualitative information about the response of individual amino acids of a protein to its interactions with ligands. Line shapes derived from ^{15}N-HSQC spectra recorded for different steps of a ligand titration yield both kinetic constants and insight into mechanisms by which the ligand binds. Here we have analyzed line shapes for 37 signals of amino acids of the N-terminal src homology 2 domain (N-SH2) of the 85 kDa subunit of phosphatidylinositol 3-kinase (PI3-K) upon binding of phosphotyrosine (ptyr)-containing peptides. Kinetic rates at individual amino acids of the SH2 varied throughout the structure. For a subset of SH2 residues, the fine structure of the NMR line shapes indicated slow motions induced by the presence of small amounts of the ligand. These complex line shapes require one or more additional conformational states on the kinetic pathway. Modeling of the observed ligand interactions suggests a quasi-allosteric initial binding step. N-SH2 mutants with altered ligand affinity or specificity were also examined. Analysis of their line shapes revealed three distinct classes of mutants with different kinetic behaviors.

Differential line broadening of one-dimensional NMR data is a common tool for studying chemical kinetics. It has most often been employed to study chemical exchange or conformational averaging of small organic molecules. For large biomolecules, line shape analysis has been reserved for some isolated signals, such as high-field methyl resonances (*1*). Isotope-edited two-dimensional NMR spectra offer an increased number of opportunities for analysis of differential line broadening and provide kinetic data for different positions in a protein both because of increased dispersion and because chemical shift perturbations of both nuclei become accessible to analysis. This has made line shape analysis applicable to problems of protein folding (*2*) and ligand binding kinetics for larger proteins (*3*). Line shapes recorded for a protein upon ligand binding contain valuable information about the binding rates and mechanism (*4*, *5*). They are most easily interpreted for fast exchange on the NMR time scale for an individual nucleus (here ^{1}H or ^{15}N). Sudmeier (*6*) has shown theoretical line shapes for ligand titrations where line shapes depend on the amount of ligand added. However, line shapes in slow exchange have also been analyzed assuming complex binding mechanisms (*3*). For quantitative line shape simulations, the proper choice of a suitable kinetic model is crucial. We have recently described an effective method for calculating line shapes derived from two-dimensional NMR spectra and have demonstrated the complexity of line shapes that can arise from certain kinetic mechanisms (*7*). Here we have used differential line broadening to study binding kinetics for individual amino acids of the N-terminal SH2[1] domain of the p85 subunit of PI3-kinase (PI3-K).

PI3-K is an enzyme broadly important for trafficking and cell signaling (*8*−*18*). Mitogenic signaling (*19*, *20*), vesicle trafficking (*21*, *22*), cell movement (*23*), rearrangement of cytoskeletal actin (*24*), and chemotaxis (*25*) are all normal cell functions where PI3-K plays an important role. Activation is also associated with acute stimulation such as platelet activation by thrombin (*26*, *27*), stimulation of neutrophils by fMet-Leu-Phe (*28*), and stimulation of phagocytosis (*29*). PI3-K pathways have important roles in oncogenesis. The original interest in the enzyme came from its association with oncogenes such as v-src and polyoma middle T (MT) (*30*). Retroviruses expressing mutant forms of PI3-K or its downstream target Akt can induce tumors (*31*, *32*). In the case of middle T, activation of PI3-K is required for tumor formation at sites such as kidney and is critical in others such as breast (*33*). Besides its role in stimulation of cell growth, PI3-K has a role in preventing apoptosis in a variety of cell types (*34*, *35*). Finally, PI3-K activation is also associated with tumor invasion (*36*).

† This work was supported by the Deutsche Forschungsgemeinschaft, by the NMR Large Scale Facility Frankfurt (UNIFRANMR), by NIH Grants CA34722 and CA50661 (to B.S.), and by a NATO collaborative research grant.

* To whom correspondence should be addressed. Telephone: 49-(0)69-79829623. Fax: 49-(0)69-79829632. E-mail: ugunt@bpc.uni-frankfurt.de.

‡ J. W. Goethe University.

§ Tufts University.

[1] Abbreviations: HSQC, heteronuclear single-quantum coherence; FID, free induction decay; CPMG, Carr−Purcell−Meiboom−Gill pulse sequence; PDGFr, platelet-derived growth factor receptor; MT, polyoma virus middle T antigen; p85, 85 kDa subunit of phosphatidylinositol 3-kinase; PI3-K, phosphatidylinositol 3-kinase; SH2, Src homology 2 domain; N-SH2, N-terminal src homology 2 domain of p85; ptyr, phosphotyrosine.

10.1021/bi0202528 CCC: $22.00
Published on Web 09/06/2002

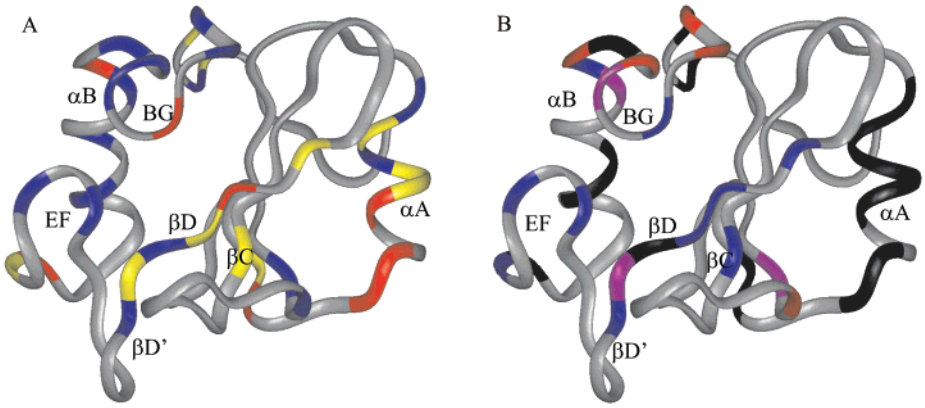

FIGURE 1: Structure of the p85 N-SH2. (A) Colored residues indicate those residues for which line shapes were analyzed from two-dimensional ^{15}N-HSQC spectra. The three colors indicate three regions of lifetimes: $k_{off} > 1000\ s^{-1}$ (red), $650\ s^{-1} < k_{off} \leq 1000\ s^{-1}$ (yellow), and $k_{off} < 650\ s^{-1}$ (blue). The description of structural elements follows the nomenclature introduced by Eck (*68*). (B) Colors indicate different types of line shapes for individual residues of the protein. Black is for residues for which line shapes can be described by second-order binding according to $P + L \rightleftharpoons PL$. From blue to violet to red, line shapes show different levels of complexity as described in footnote a of Table 1 [+++ (red), ++ (violet), and + (blue)].

Intracellular trafficking of PI3-K is mediated by the binding of Src homology 2 (SH2) domains. Binding of SH2s to tyrosine-phosphorylated sequences of proteins such as the PDGF receptor (PDGFr) (*37*−*39*) or polyoma MT (*40*) is part of many processes of cell regulation (*41*−*44*). In the case of MT, for example, phosphotyrosine residue 315 interacts with the SH2s of the p85 subunit of PI3-K. X-ray diffraction and NMR have established the structure of a number of SH2−tyrosine phosphopeptide complexes (for a review of SH2 structures, see ref *45*), including the SH2s of PI3-K (*3*, *46*−*50*). All SH2s can be described as a central triple antiparallel β-sheet flanked by smaller β-sheets and two α-helices (Figure 1). For most SH2s, the specificity of the interaction with phosphopeptides is determined by the first (+1) and third (+3) residues after the phosphotyrosine (ptyr). In the case of the more N-terminal SH2 of PI3-K (N-SH2), preferred residues at position +1 are M, V, I, and E, while M is the preferred residue at position +3 (*51*). Different classes of SH2s reveal different patterns of specificity. In some cases, changes in a single amino acid of the protein can alter its specificity. Changing the βD5 from I to Y, for example, has been shown to change the specificity of the N-SH2 of PI3-K (*52*).

The goal of this work has been twofold: to study how SH2s function and to expand the ways NMR analysis can be used to study ligand interactions. We have examined the interactions of tyrosine-phosphorylated peptides matching middle T or PDGF receptor sequences known to bind PI3-K with the N-SH2 of the p85 subunit. Using ^{15}N-labeled protein and ^{1}H,^{15}N-HSQC spectra, 37 of 110 amino acids were accessible to differential line broadening analysis. We have compared the behavior of different peptide ligands and mutant SH2s. Qualitative examination of the line shapes shows dramatic differences in the behavior of individual residues. These showed clear evidence for structural rearrangements on a millisecond time scale induced by the binding process. Although such line shapes were too complex to be fully simulated, they provide information about the mechanism of the interaction for individual amino acids. Of particular interest, line shape measurements could be used to distinguish the structural effects of different kinds of mutations. In addition, titration experiments showed that the interactions of different SH2 residues with the ligand are characterized by different off-rates. This is a form of dynamics measurement that provides information complementary to CPMG measurements (*53*, *54*) that can be used to calculate exchange rates on a microsecond to millisecond time scale.

MATERIALS AND METHODS

The wild-type pGEX3X−GST−N-SH2 construct (amino acids 321−434) and the methods used to produce SH2 for NMR analysis were described previously (*55*). Binding properties of the mutants P395S and P427L were also reported previously (*56*). The mutant I381Y (*52*) was constructed by site-directed mutagenesis using the oligonucleotides 5′-GGGGGAAATAACAAATTATATAAAATATTTCATCGAGAT-3′ and 5′-ATCTCGATGAAATATTTTATATAATTTGTTATTTCCCCC-3′ as previously described (*57*). ^{15}N-labeled SH2 has been prepared using either rich medium (Celtone U, Martek) or minimal medium prepared with $^{15}NH_4Cl$ (Cambridge Isotope Laboratories). Factor Xa (Haematologic Technologies) was used to cleave the SH2 from the fusion protein. The SH2 was further purified by gel chromatography (Superdex 75). The pH of both the SH2 and the ligand solution was adjusted to 6.8 by careful titration with HCl or NaOH. Phosphopeptides were synthesized and HPLC purified by the Tufts Protein Chemistry Facility (*55*). Peptides that were used were EEEpYMPME-NH_2 from the middle T sequence around the tyrosine phosphorylation site at residue 315 where PI3-K binds and SVDpYVPML-NH_2 from the PDGF receptor sequence at the residue 751 binding site. The purity of peptides was evaluated using MALDI mass spectrometry. The purity of proteins was judged by gel chromatography and the fact that ^{1}H,^{15}N-HSQC spectra exhibited a unique set of assigned signals. Concentrations of the protein and peptide were measured by UV absorption at 279 nm [using extinction coefficients of 610 $M^{-1}\ cm^{-1}$ for ptyr in peptides and 1522 $M^{-1}\ cm^{-1}$ for tyr in the SH2 (*58*, *59*)]. Concentrated solutions of peptides were made to avoid dilution of the protein upon addition of peptide. The typical volume added in one titration step was 10−15 μL in a total volume of ∼250 μL. After addition of the peptide, the homogeneity of the static magnetic field was readjusted and the tuning of the probe circuit was checked.

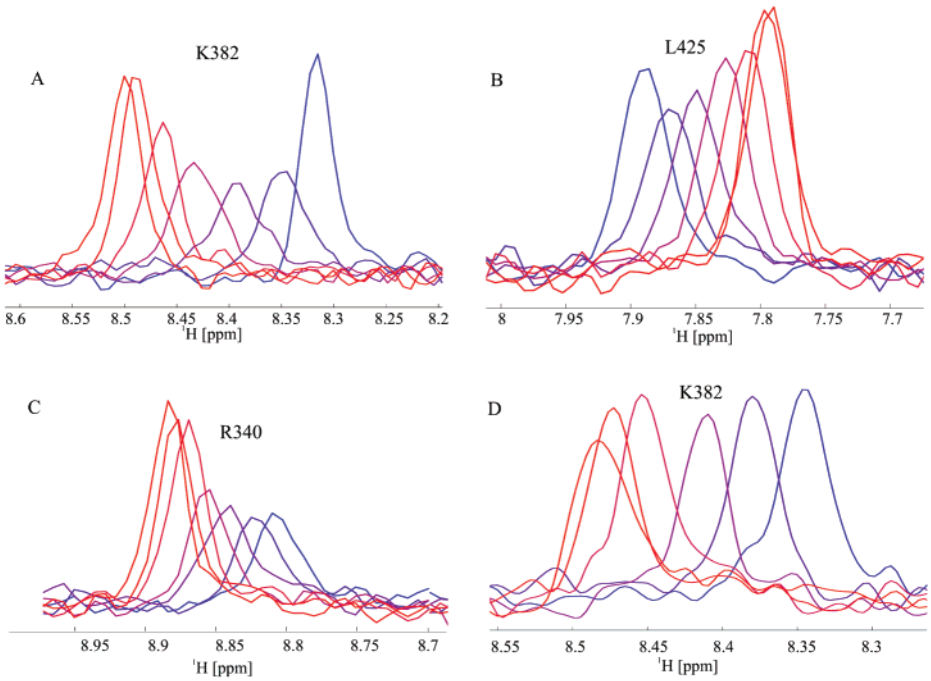

FIGURE 2: Line shapes in the proton dimension of HSQC spectra recorded for a titration of the p85 N-SH2 with EEEpYMPME-NH_2 (MT peptide) (A−C) and phosphotyrosine (D). All titrations proceed from blue (free SH2) to red (SH2 complex).

HSQC spectra were recorded on BRUKER AMX 500 (wild-type SH2) and DMX 500 (SH2 mutants) spectrometers with 2048 data points in the ^{1}H dimension, and a minimum of 256 increments in the ^{15}N dimension. Spectra used for line shape analysis in the ^{15}N dimension were recorded with 700−1024 points in the ^{15}N dimension. Spectra were processed and line shapes extracted from two-dimensional spectra using NMRLab (*60*). Gaussian broadening was employed prior to Fourier transformation with LB −5 and GB 0.05 in the incremented dimension and LB −3.0 and GB 0.03 in the recorded dimension.

Line shape calculations were performed as described in ref *7* using software written for MATLAB (The Mathworks). The software was written to calculate the time domain signal for sections of HSQC spectra. Line shapes were fitted assuming second-order binding according to $P + L \rightleftharpoons PL$ using optimization routines available for MATLAB. The accuracy of such simulations depends very much on the rates. For example, in very fast exchange, lines will hardly be broadened and the intensity of lines will hardly be reduced during the titration. For a peak separation of 500 Hz, lines vary little for a k_{off} of >5000 s^{-1}. For this reason, the rate determined from such line shapes has a large error. A detailed discussion of the error of line shape simulations is found in the Appendix. In this work, we decided to group off-rates in the fast exchange regime into three categories ($k_{off} > 1000$ s^{-1}, 650 s^{-1} $< k_{off} \leq 1000$ s^{-1}, and $k_{off} < 650$ s^{-1}).

RESULTS

Previous work has identified residues in the p85 N-SH2 that show chemical shift perturbations upon binding of tyrosine-phosphorylated middle T or PDGF receptor peptides (*55*). These chemical shift changes defined SH2 residues that respond to the binding of the phosphotyrosine (ptyr) or the first residue (+1) or the third residue (+3) C-terminal to the ptyr of the ligand. In binding experiments with a peptide (EEEpYMPME-NH_2) derived from MT antigen, 51 of 108 SH2 residues showed chemical shift perturbations at least 2−3 times greater than the line width. Because spectral overlap made evaluation of some of these signals impractical, only 37 residues could be analyzed in greater detail. Figure 1A shows a ribbon diagram of the p85 N-SH2 highlighting the 37 residues for which line shapes were studied. All regions of the SH2 are represented, including residues expected to interact with the phosphotyrosine (R340 and R358), with the +1 residue (K379 and I381), and with the +3 residue (I381, F392, and K419) in the ligand peptide as well as residues which are not directly involved in ligand interactions (F384, E345, K346, and L347).

The line shapes of individual residues in the ^{15}N-HSQC spectra were analyzed by examining cross sections of peaks during titration with ligand. When protein is titrated with ligand, two general types of behavior can be expected for NMR line shapes of signals that have different chemical shifts in the free protein and in the protein complex. In the case of slow exchange on an NMR time scale ($k/\Delta\nu < \pi/\sqrt{2}$), where k is the exchange rate and $\Delta\nu$ the frequency separation of the exchanging signals, the intensities of the two peaks of free and complexed forms will be proportional to the relative amount of free protein and protein complex present in the mixture. No true examples of slow exchange between the free protein and the protein−ligand complex were observed for interactions of the MT peptide with the N-SH2. Complex behavior was observed for E411 because the signal of the free protein showed a minor second component in slow exchange, while only one signal was present in the MT complex (not shown). For fast exchange rates ($k/\Delta\nu > \pi/\sqrt{2}$), a single peak with an intermediate chemical shift is observed at each step in the titration. Examples of this sort of behavior are shown in Figure 2. The intermediate case of coalescence ($k_{coal}/\Delta\nu = \pi/\sqrt{2}$) will never occur simultaneously for all steps of a titration be-

Table 1: Line Shapes of Signals of the p85 N-SH2 during a Titration with the MT Peptide

amino acid	signal comp[a]	K_{ex}[b]	k_{off} (s^{-1})[d]	amino acid	signal comp[a]	K_{ex}[b]	k_{off} (s^{-1})[d]
W335			950 [−190 + 290]	F392	+	0.9	550 [−60 + 90]
G336		0.8	>2000[f]	D394	+	0.8	540 [−100 + 170]
S339		0.85	1120 [−220 + 310]	T397	+		950 [−150 + 210][e]
R340		0.7	>1500 [f]	F398			>2500[f]
Y343			1900 [−390 + 990]	L404			380 [−120 + 280]
N344		0.85	680 [−110 + 130]	N406		0.88	610 [−210 + 480]
E345			710 [−90 + 120]	R409	++	0.6	260 [−50 + 70]
K346			640 [−90 + 120]	N410	+	0.92	2660 [−410 + 340]
L347			770 [−100 + 140]	E411	+++		-
R348		0.95	250 [−60 + 240]	S412	+++	0.75	600 [−120 + 160][e]
R358	++		470[f]	A414	+++	0.65	400 [−60 + 80][e]
A360	+++		300 [f]	Q415	++	0.85	500 [−60 + 90][e]
T369	+		980 [−140 + 200]	N417	*c*		1910 [−660 + 1850]
K379	+		930 [−100 + 120]	K419	+++	0.85	550 [−120 + 150][e]
I381	+[c]		1210 [−130 + 170]	D421	+++	0.75	400 [−90 + 140]
K382	+		650 [−90 + 120]	V422		0.75	830 [−180 + 280]
I383			590 [−120 + 200]	L424			480 [−90 + 130]
F384	++		920 [−180 + 260]	L425		0.9	910 [−220 + 380]
H385	+		560 [−80 + 110]				

[a] Qualitative classification of line shapes: blank, lines could be simulated assuming a two-state model; +, minor shoulders in one or two lines of the titration; ++, line shapes as described for F384 with shoulders in multiple lines of the titration; +++, significant distortion of lines during the titration with disappearing signals. [b] For K_{ex}, line shapes showed changes in intensity similar to that of R340 that required the consideration of an external equilibrium (*7*). [c] The line in the first titration step showed a shoulder. A line shape simulation considering this extra feature yields a higher value for k_{off}. [d] Off-rate with error estimation calculated as described in the Appendix in parentheses. [e] Error estimation failed because of the complexity of line shapes. For these lines, off-rates are very uncertain because a two-state mechanism must be questioned. [f] Upper error estimation not possible because the signal is not altered for larger rates.

cause one of the effective rates depends on the ligand concentration (*7*).

Figure 2A−D shows examples of fast exchange that were observed, where lines (in the ^{1}H dimension) from a two-dimensional HSQC spectrum are displayed in colors from blue to red for successive steps of the titration. The ribbon diagram of Figure 1B summarizes the residues that showed simple two-state behavior in black. R340 (Figure 2C) represents a variant in this category of signals because the line in the free protein has a significantly smaller intensity than that in the complex. Table 1 lists other residues that showed this type of behavior. Several possible explanations for this behavior have been explored. Relaxation measurements exclude the possibility of an exceptionally high transverse relaxation rate R_2 for this residue (U. Günther, unpublished data). A second possibility is that slow exchange with one or several other conformers that are unable to bind ligand causes the reduced signal intensity of the free state. This is unlikely because CPMG relaxation measurements do not show increased mobility on a millisecond time scale (U. Günther, unpublished results). A plausible explanation would be a reduction in hydrogen exchange rates upon binding. This possibility is generally supported by the observation that most residues for which the intensity of the line in the free state was reduced are located in loop regions which are exposed to the solvent. Also, changes in hydrogen exchange rates have previously been shown for the N-SH2 and interpreted to reflect changes in SH2 stability (*61*). Hydrogen exchange rates were measured for the free wild-type SH2 and for the SH2 complexed to a MT peptide (Figure 3). Clearly, hydrogen exchange rates are high in loop regions and low in the central parts of the β-sheet. However, the signal of R340 is in fast exchange with the solvent and cannot be detected immediately after addition of D_2O in either the free or the complexed SH2. While none of these results explain the observed changes in signal intensity between the

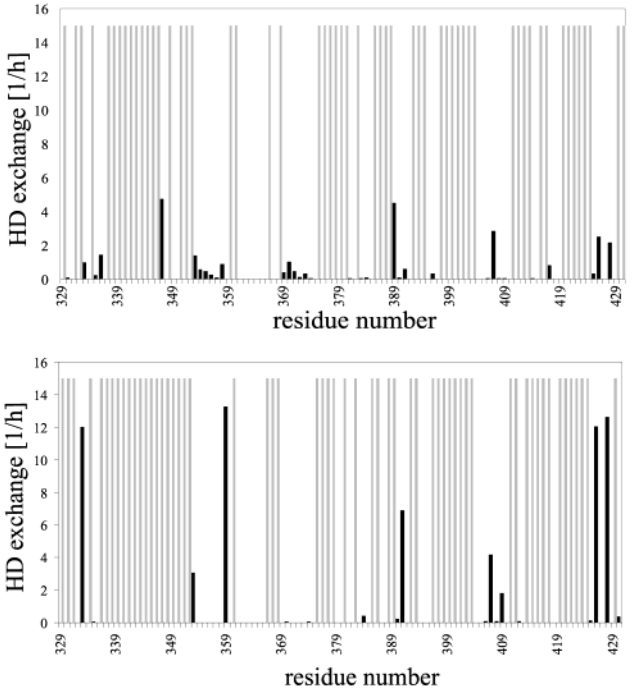

FIGURE 3: Hydrogen exchange rates for the p85 N-SH2 determined by recording HSQC spectra after dissolving the lyophilized protein in D_2O. Free SH2 (top) and SH2 complexed to the MT peptide (bottom). Grey bars indicate residues which exchanged too fast to be observed in D_2O.

free and complexed SH2, we favor the possibility of hydrogen exchange on a faster time scale, not accessible in simple deuterium exchange experiments.

In contrast to residues that showed only a single peak at intermediate chemical shifts during titration, many other residues exhibited more complex line shapes (shown in red on the ribbon diagram of Figure 1B). The most interesting result was the appearance of signal shoulders indicative of multiple long-lived states at some point during the titration

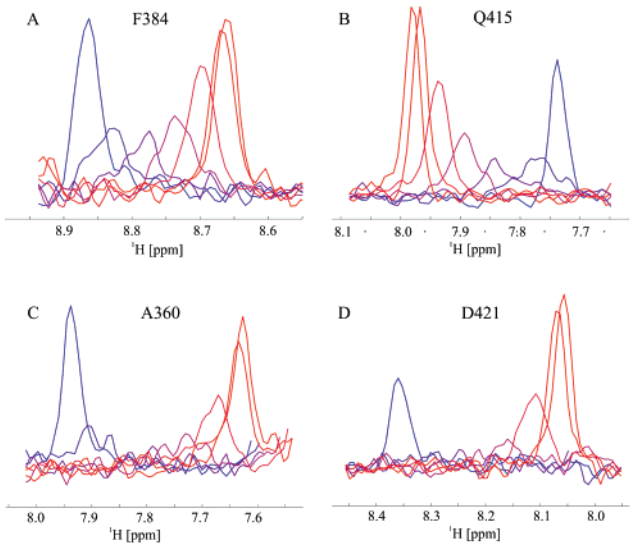

FIGURE 4: Line shapes showing complex behavior for four different residues in a titration of the p85 N-SH2 with the MT peptide. Lines proceed from blue to red for increasing concentrations of the added peptide.

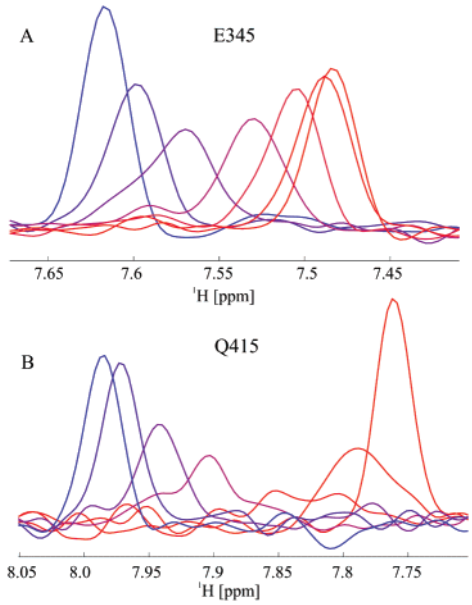

FIGURE 5: Line shapes for the titration of the p85 N-SH2 with the PDGFr peptide (SVDpYVPML-NH_2).

where only a single peak was observed for free or fully complexed SH2. An example of this can already be seen in Figure 2A, where the titration step of K382 (i.e., the third line) showed two minor shoulders.

Figure 4A depicts the striking example of F384, where several titration steps showed signals with two to three shoulders. The shoulders disappeared again in signals toward the end of titration. Q415 (Figure 4B) in the BG loop showed very similar line shapes. Signal component analysis on the FID proves that these signals are periodic in time and thus not noise-related artifacts. An even greater effect was observed for A360 (Figure 4C) and D421 (Figure 4D). Shoulders were clearly observed, for example, in the third and fourth titration steps from the end. In cross sections recorded at an earlier stage of the titration, the heterogeneity induced by ligand binding was so great that the signal was essentially lost. Importantly, none of these residues showed an indication of shoulders in the free SH2. Also, conformational averaging on a slow time scale should also be observed in high R_2/R_1 ratios and in R_2 dispersion determined by CPMG sequences with variable echo times. Neither measurement supports significant millisecond mobility in the free SH2 (U. Günther, unpublished results).

To test whether the effects observed were specific to the middle T ligand, a peptide titration was also carried out for the peptide SVDpYVPML-NH_2, a sequence matching the tyrosine phosphorylation site at residue 751 of the PDGF receptor. Previous competition experiments showed that this peptide was only slightly lower in affinity than that from MT [IC_{50} = 13.4 vs 8.3 mM (*55*)]. However, peptide selection experiments for the SH2 showed that V is not as favored as M in the +1 position (*56*). Differences in chemical shift changes upon PDGFr titration changed the subset of residues that could be analyzed. For example, K382 shifted only slightly when the PDGFr peptide was added. Analysis of chemical shift perturbations showed that this peptide had an effect on K379 and L420, two residues which are important for the interaction of the β-sheet and the BG loop. L420, for example, showed a chemical shift in the opposite direction when PDGFr peptide was added, but the line shape pattern is the same as for the MT peptide. Despite these differences in the titration, the behavior of the line shapes appeared to be similar. Residues which showed complex behavior for MT also showed complex behavior for PDGFr. Figure 5 shows two examples, E345 and Q415. Line shapes for E345 were close to those expected for two-site exchange. A small shoulder in one titration step suggests that a slow rearrangement may play a role during the titration. The same type of shoulder was also observed for the neighboring residue, K346. Line shapes for Q415 showed complex features similar to those observed for the MT peptide.

Line Shape Analysis Shows Differences among Individual SH2 Residues in Local Off-Rates. Line shapes contain quantitative as well as qualitative information. Protein−ligand interactions characterized by very high off-rates and consequently low affinity show peaks with similar intensities and line widths for different concentrations of ligand in a titration. An example of this type of interaction is shown in Figure 2D for K382 in a titration with ptyr. For the K382−ptyr interaction, very high off-rates were expected for the low affinity of ptyr ($K_D \approx 1$ mM) because $k_{off} = K_D k_{on}$.

High-affinity interactions, such as the interaction of the MT peptide with K382 (Figure 2A), were characterized by line broadening and decreased peak intensities during the titration. Quantitative analysis can be performed on this kind of line shape data using simulated line shapes to estimate k_{off}, the local off-rate, on a residue by residue basis. Line shapes of this type can be simulated assuming a model with second-order binding ($P + L \rightleftharpoons PL$). The mutual effect of line shapes of the two spectral dimensions had to be considered for the calculation because the chemical shifts of both nuclei, ^{1}H and ^{15}N, were affected by ligand binding (*7*). For residues such as R340, the reduced signal intensity of the free state can be handled in line shape simulations by adding an external equilibrium for the free state as described previously (*7*). This procedure accounts for any type of slow exchange which affects the line shape of the amide ^{15}N and

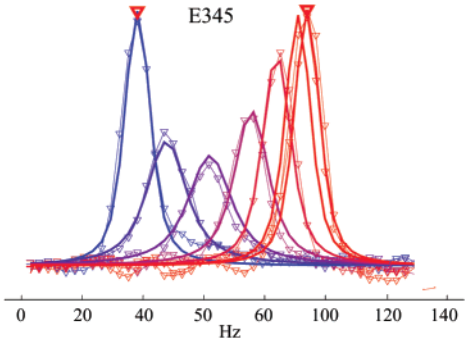

FIGURE 6: Experimental signals (lines with ▽ from blue to red) and simulated line shapes (—) for the E345 residue in a p85 N-SH2−MT titration.

^{1}H nuclei, including exchange with the solvent or between different conformers. An example of a simulation is shown for the interaction of the MT peptide with E345 (Figure 6). The simulation gave a value of 710 s^{-1} for the off-rate k_{off}. For the MT peptide interaction with K382, a k_{off} of 650 s^{-1} was obtained, consistent with the micromolar affinity of the MT peptide and diffusion-controlled on-rates ($k_{off}/K_D = 650\ s^{-1}/10^{-6} \approx 10^9\ s^{-1}$). This is equivalent to a lifetime τ_{off} ($=1/k_{off}$) of ≈1.5 ms for the bound state (PL). For the interaction of ptyr with K382, line shape analysis yields a k_{off} value of $>10^4$ (higher rates cannot be distinguished for the chemical shift differences observed for ptyr binding). If diffusion-controlled on-rates are assumed, k_{off} cannot be higher than $K_D k_{on}$ ($10^{-3} \times 10^9\ s^{-1} = 10^6\ s^{-1}$). The same behavior and similarly high off-rates were observed for all other residues of the SH2 which titrate upon adding ptyr (S339, E345, R358, D359, A360**,** T369**,** L370, T371, I381, K382, I383**,** H385, and F392).

Table 1 lists the results of a line shape analysis for 37 residues titrated with the MT peptide. Lifetimes τ_{off} varied between approximately 0.4 and 4 ms, suggesting that the interaction with the MT peptide is not uniform for all residues of the protein. The line shapes can be roughly classified in three groups: $k_{off} > 1000\ s^{-1}$, $650\ s^{-1} < k_{off} \leq 1000\ s^{-1}$, and $k_{off} < 650\ s^{-1}$. The colors of Figure 1A indicate the calculated off-rates for the 37 residues listed in Table 1. Off-rates of all three categories were observed in different parts of the protein. The differences in off-rates were not connected to ligand interactions in any simple way. Some residues important for ligand binding such as H385 and I383 showed particularly low off-rates (590 and 560 s^{-1}), i.e., long lifetimes of interaction (1.7 and 1.8 ms). Relatively long lifetimes were also observed for residues in the EF loop (F392 and E394). F392 is directly involved in interactions with the peptide. However, D394 is not and points away from the molecule. It seems likely that lifetimes are correlated to concerted rearrangements in the protein. Side chain contacts, for example, between the side chains of F384 and F392, may be important for cross talk between different structural elements of the protein. For one group of adjacent residues, N344, E345, and K346, off-rates were relatively low (640−710 s^{-1}), despite the fact that these residues do not play a major role in the interaction with the ligand. Their chemical shift changes must be secondary effects not caused by direct interactions with the ligand. Astonishingly, the off-rate for I381 is $>1000\ s^{-1}$, although this residue is known to interact with the +1 residue of the bound phosphopeptide.

Line Shape Analysis Distinguishes Different Classes of Mutants. Many mutant N-SH2s with differing properties are available for line shape analysis (*56*). Three, P395S, P427L, and I381Y, were selected to compare to wild type both to understand better the wild-type line shapes and to see how line shape analysis could be used to provide insight into the behavior of the mutants.

I381. The βD5 residue is thought to control specificity at the +1 position. Mutation of βD5 from I381 to Y resulted in a reduced affinity for peptides with a pYMPM sequence and an increased affinity for peptides of the type pYEEI (*52*). Figure 6 shows representative line shapes for the I381Y mutant, which binds MT with low affinity. The line shapes shown for A360 and for E345 are representative examples of line shapes observed for this mutant which showed typical features for low affinity with very high off-rates. Lines showed no increased line width and therefore no reduced intensity in intermediate signals during the titration. This behavior is the same as that observed for ptyr with wild-type SH2 (Figure 2D). Some reduction in signal intensity in conjunction with some fine structure in line shapes was seen in the first titration step (second spectrum) for A360. However, shoulders in lines were very much reduced, and the amount of reduction of the overall signal intensity is minimal compared to that observed for the wild-type SH2.

P395S, another mutant with altered specificity, is defective in binding MT but is unaffected in its ability to bind the PDGF receptor (*56*). The mutation is in the EF loop and causes a loss in the ability to select methionine at the +3 position. At the same time, binding experiments established that the mutant prefers valine at +1 whereas the wild type prefers M, V, I, and E, in that order, at the +1 position. This change in selectivity explains why P395S retains the ability to bind PDGFr (pYVPM) while losing affinity for MT (pYMPM). The assignments of P395S and calculated structures will be presented elsewhere (U. Günther, in preparation). Here we show how line shape analysis of titrations with the MT peptide provided insight into the altered behavior of the P395S mutant. With regard to changing the ligand sequence from MT to PDGFr for the wild-type SH2, mutation of the SH2 had some effect on which residues could be subjected to line shape analysis. F392, close to the site of the position 395 mutation, showed a smaller chemical shift perturbation; T397 disappeared completely, and D394 and L396 had relatively weak signals. Titration of P395S with the MT peptide showed striking changes in the nature of the lines from that observed with the wild type. As seen in Figure 8A for I381 in the nitrogen dimension and in Figure 8B for K382 in the proton dimension, the intermediate lines in the titration seemed to "bunch" (black bar) as the titration proceeds. Compared to the behavior of the wild-type SH2, addition of more ligand at intermediate steps for most residues in the titration with the MT peptide results in only a small change in the chemical shift. In Figure 8A, intermediates seemed to be bunched around 124.7 ppm and showed multiple signals in the spectrum of step 7 in the titration at a ^{15}N chemical shift of ∼124.7 ppm, indicative of a slow exchange process on the reaction pathway:

$$P + L \underset{k_{off}}{\overset{k_{on}}{\rightleftharpoons}} PL^* \overset{[L]}{\rightleftharpoons} PL$$

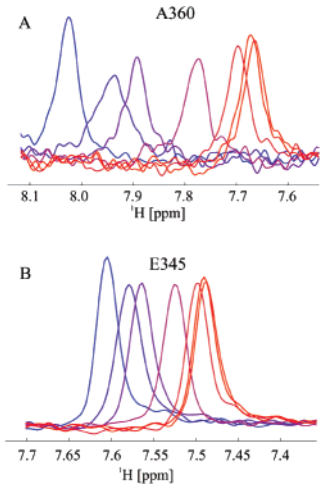

FIGURE 7: Cross sections from HSQC spectra in titrations of the I381Y mutant of the p85 N-SH2 with MT peptide.

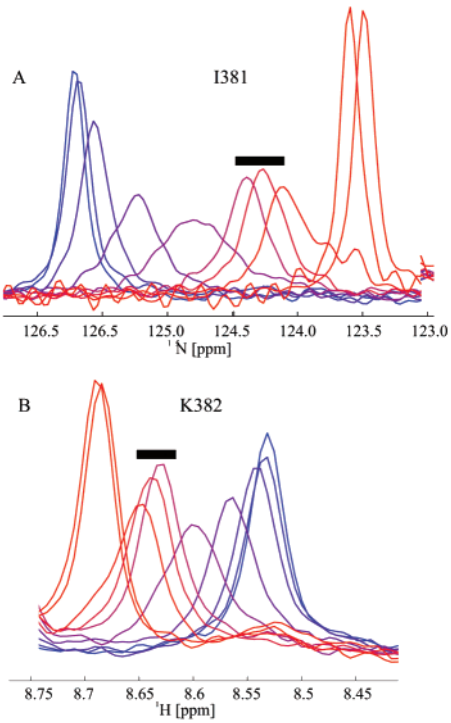

FIGURE 8: Sections from HSQC spectra in a titration of P395S with the MT peptide. Bars indicate signals which are bunched in subsequent spectra of the titration.

The simplest interpretation of this behavior is that the mutant SH2 experiences fast initial binding of L (on a microsecond time scale) associated with chemical shift changes reflecting the PL*/PL ratio followed by a slow conformational rearrangement between PL* and PL. However, the PL*/PL ratio clearly depends on the ligand concentration.

A second feature of the P395S titration was equally striking. Shoulders comparable to those observed for A360 or D421 for the wild-type protein were not observed in the first steps of the titration. This is obviously different than for the wild-type N-SH2 for which multiple shoulders were observed in intermediates in titration with either MT or PDGFr peptides. A reasonable interpretation of this observation is that the intermediates ordinarily seen in the wild type are not induced in the P395S mutant. It seems likely that this failure contributes to the lower affinity.

P427L is a mutant which eliminates binding of either MT or PDGFr (*56*). It has low affinity for the MT or the PDGFr peptides ($K_D \approx 1$ mM). These results were superficially unexpected because the location of the mutation is in the very end of the SH2, remote from the binding pockets of the SH2. Chemical shifts in HSQC spectra indicated that the mutation causes changes in the N-terminus, in the central β-sheet, in the C-terminal residues of αB, and in BG (Figure 9A). For a large segment in BG, no signals could be identified in either the free protein or the protein−MT complex. This can be ascribed to flexibility in this region of the protein and indicates that the back side contributes stability to the structure.

Figure 10 shows line shapes of P427L for a titration with the MT peptide. For some residues such as R340 (Figure 10A), lines were clearly broadened during the titration despite the low affinity for the peptide. Similar line shapes were observed for other residues in αA (S339 and E345) and in EF (S393 and D394, cyan in Figure 9B). More striking behavior was observed for I381, as shown in HSQC spectra at different stages of a titration with the MT peptide (Figure 10B) and in cross sections in Figure 10C. Cross sections for I381 (Figure 10C) show complex line shapes, a common feature of many residues of P427L. Inspection of line shapes in intermediate spectra during the titration showed that most signals have four to five components. The signal seemed to almost disappear into the background at intermediate stages of the titration. Other residues as shown in red in Figure 9B gave results similar to those for I381. This behavior was completely unexpected for low-affinity binding and was different from the line shapes observed for the low-affinity interaction of ptyr and wild-type SH2.

P427L also showed one additional new feature in its titration. Despite the presence of multiple conformers, most signals move on a straight line in the two-dimensional HSQC spectra with increasing ligand concentrations. However, in P427L we observe at least one signal (F392) where initial chemical shift changes occur in the ^{15}N dimension but the final signal appears with a strong change of both frequencies (0.2 ppm for ^{1}H and 0.65 ppm for ^{15}N, not shown). The signal seems to move "around a curve" in the two-dimensional HSQC spectrum. This behavior requires multiple long-lived intermediates which are not seen in intermediate spectra during the titration.

DISCUSSION

While structural analysis can elucidate the structure of protein−ligand complexes, understanding the mechanisms by which proteins and ligands interact remains a most challenging problem. Similarly, rationalizing the behavior of mutant forms of proteins is often highly problematic. Here we have used analysis of NMR line shapes to study binding properties of wild-type and mutant SH2s. A major advantage of this approach over other techniques that have been used to study binding kinetics is that differential line broadening using isotope-edited two-dimensional NMR spectra provides kinetic data for different positions in a protein. In addition, the shapes of lines reveal more detailed information about the processes involved in protein−ligand interaction. The N-SH2 of p85 of PI3-K is attractive for these kinds of studies

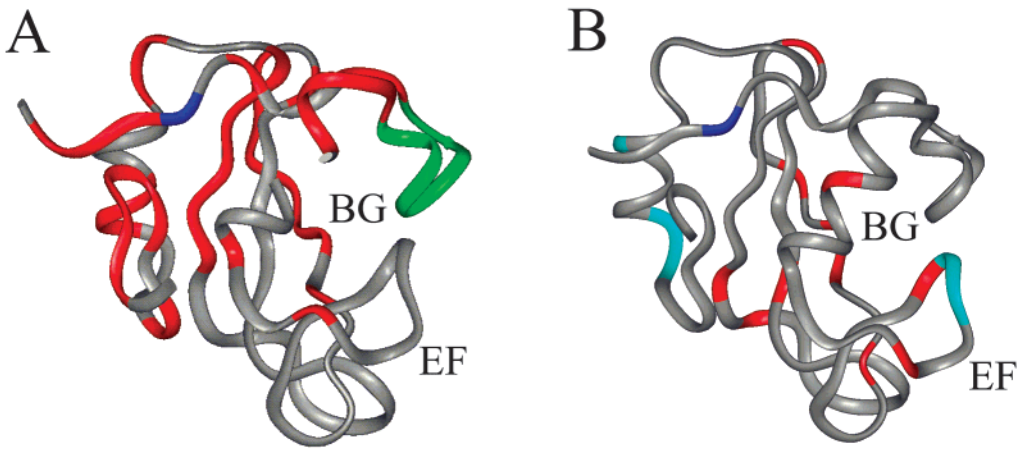

FIGURE 9: Structure of the p85 N-SH2 shown at a 90° angle compared to Figure 1. Colored residues indicate altered chemical shifts in P427L. The mutation site is displayed in blue. (A) Red is for residues for which the chemical shift was altered in P427L compared to that in the wild type. Green is for residues which could not be assigned in the P427L mutant. (B) Types of line shapes for residues which change their chemical shift in the P427L mutant. Red is for signals that exhibit a large number of shoulders in multiple titration steps (e.g., I381). Cyan is for signals showing relatively smooth lines comparable to those of R340 (Figure 10A).

for many reasons. PI3-K is a critical enzyme for cellular signal transduction. Both interesting mutants and ligands are available for studying binding properties. Structural studies using both X-ray and NMR are available for comparison to the results of the line shape analysis. Most importantly, good spectral dispersion permitted analysis of a large number of residues distributed across the surface of the SH2. Essentially all residues that could be titrated showed fast exchange, indicating that off-rates would be on the order of 1000 s^{-1}. Finally, Hensman et al. (*3*) have studied line broadening for two of these residues (E411 and K379) of a different variant of the p85 N-SH2, pointing to the feasibility of such studies.

Complex Line Shapes. The most striking aspect of the N-SH2 ligand interaction is the existence of multiple species in the intermediate steps of the titration. Heterogeneity induced by ligand binding was observed for many residues across the protein (Figure 1B). This could be seen as shoulders, in the case of F384 or R358, or in the apparent loss of the signal at intermediate steps in the case of A360, Q415, K419, or D421. Most of these residues are located in loop regions or interact with loops through their side chains. For example, the side chain of F384 interacts with F392 in the EF loop. In all, signals for at least 20 of 37 residues exhibited shoulders in intermediate spectra during the titration.

How can the fine structure of intermediate signals in a ligand titration be explained? Somewhat similar effects have been reported previously in one-dimensional spectra for helix−coil transitions of poly-*β*-benzyl L-aspartate and in ligand binding to RNase or staphylococcal nuclease [see Sykes et al. (*4*) for a review]. Sample heterogeneity has been suggested as one possible explanation for shoulders in NH and C^{α} peaks in the helix−coil transitions. However, this does not appear to be a likely explanation here. The titrations for the wild-type protein are virtually complete at a 1:1 stoichiometry because of the high affinity. Sequence heterogeneity of the ligand is unlikely because it is not detected via HPLC or MALDI of the peptides and because degradation of the peptide would be expected to lead to peptides with very low affinity (millimolar) and high off-rates. Alternatively, heterogeneity of the SH2 protein might be possible if, for example, the factor Xa cleavage was not precise. However, this explanation would predict heterogeneity in the starting sample, which was not observed. Also, if this was the reason for peak shapes, effects on many more peaks, not just in loop regions, would be expected. Finally, such heterogeneity would not explain why complexity is different for different residues.

The observation of complex line shapes with multiple shoulders after ligand binding requires one or more conformational intermediates on the reaction pathway. The observation that a ligand can cause comformational equilibria has been made before. Earlier results with RNase (*62*) and staphylococcal nuclease (*63*) have suggested conformational equilibria that are affected by ligand binding. That such behavior is observed at some residues and not others suggests that different kinetic mechanisms must be considered for different positions in the SH2. Mutants that exhibited lowered affinity showed changes in this heterogeneity. For example, multiple shoulders were observed for F384 in intermediate spectra in titrations of wild-type SH2 with either MT or PDGFr peptides. However, for the low-affinity mutant P395S or I381Y, shoulders were not observed or their magnitudes significantly reduced in the intermediate steps of titrations. A reasonable interpretation for these observations is that the intermediates ordinarily seen in the wild type are not induced in the mutants. It seems likely that this failure contributes to the lower affinity.

Figure 11 considers some of the possibilities involving multiple conformations for the formation of shoulders in intermediate spectra during a titration. Initially, the idea of either parallel starting conformations (Figure 11A) or parallel intermediates (Figure 11B) might seem attractive. However, parallel starting conformations in slow exchange requires heterogeneity in the free SH2 which was not observed except for E411. The possibility that model 1A is correct but that the concentration of P_1 or P_2 is always too low to be detected can also be ruled out. If K ($=P_i/P$) is small, the concentration of the binding species P_i will always be low. This will cause line shapes which resemble those observed for slow ex-

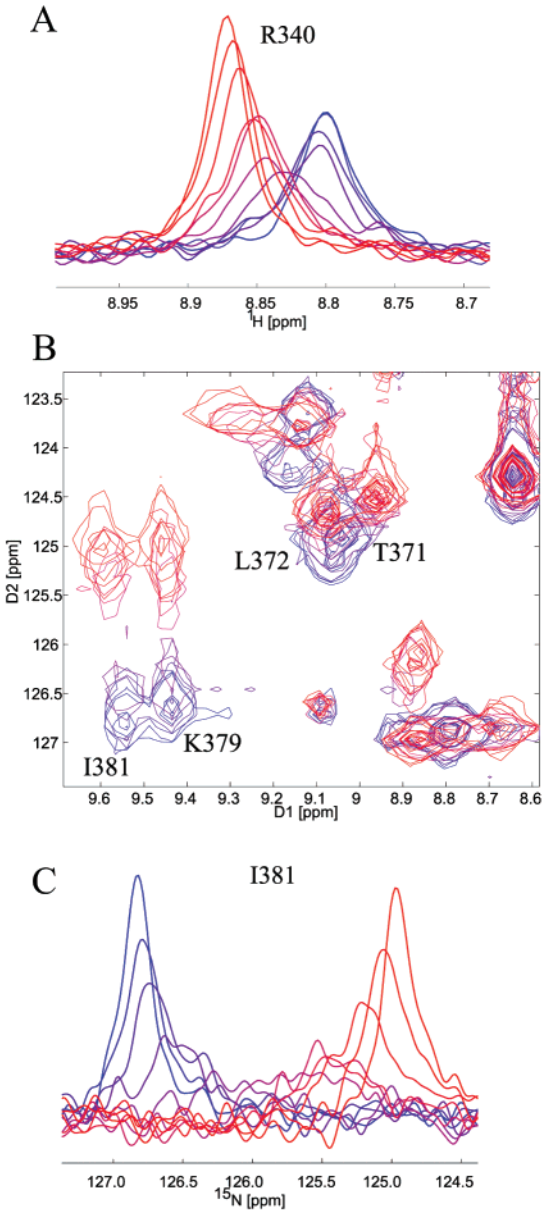

FIGURE 10: (A) Cross sections from HSQC spectra recorded for a titration of the P427L mutant with MT peptide (blue → red) for R340. (B) Section from superimposed HSQC spectra for the same titration. (C) Cross sections for I381.

change, as previously shown by the simulation of line shapes for

$$P \xrightarrow{k} P^* + L \underset{k_{off}}{\overset{k_{on}}{\rightleftharpoons}} PL$$

with only one intermediate (*7*). This is clearly not the type of line shape observed for residues such as A360, F384, K419, or D421.

An alternative mechanism (Figure 11B) describes a situation where a ligand is bound by P forming different binding products PL_i which are converted into the final product PL. For fast off-rates, peaks will move between the chemical shifts of P and PL_i in the actual binding step. The different species PL_i will convert to PL in a slow step. For this mechanism, the most complex line shapes should occur at the intermediate point where different species PL_i are present. The following conversion of PL_i into PL should show slow exchange between multiple signals. This is again not what is observed in complex line shapes of the wild-type SH2 binding MT or PDGFr peptides.

Clearly, an additional level of complexity is required to interpret some of the complex line shapes observed in our titrations. One simple possibility is that heterogeneity is induced by an encounter with the ligand (Figure 11C). In this mechanism, the formation of P_i conformations is crucial for high-affinity binding. Although P_0 may still be involved in direct interactions with the ligand (L), binding through P_i will represent major pathways. This amounts to a kind of allosteric model because the formation of binding conformations is induced by initial interaction with ligand. Allosteric effects in a single-domain signaling protein were recently described by Kern et al. by measuring dynamics of exchange between active and inactive conformations for different mutants of the signaling protein NtrC (*64*).

Such a mechanism explains why line shapes are most complex in the beginning of the titration but show a reduced amount of complexity toward the end where they are dominated by the signal of PL. The initial interaction of the protein and ligand which causes formation of binding conformers P_i must be released during the binding process because the observed stoichiometry is 1:1. In two-dimensional ^{15}N-HSQC spectra, both chemical shifts of intermediates P_i will usually be different from those of P_0.

Off-Rates. Quantitative calculations indicated that the interactions of individual residues with ligand were characterized by differences in the off-rates (Figure 1A). The distribution of apparent off-rates over the SH2 ranging from approximately 250 to 2500 s^{-1} was clearly not uniform. However, rates are not grouped in distinct regions of the protein. Except for some examples (K382, I383, I385, F392, D394, and T397) where rates of adjacent residues are in a similar range, the role of the rate for an individual residue remains a puzzle. It is, for example, not clear why the off-rate of F398 is more than twice that of its neighbor T397. One possible explanation is that the local off-rate monitored on the backbone NH group represents possible interactions of the side chain (which cause rearrangements of the local geometry, resulting in chemical shift changes). This is a plausible explanation for T397 and F398 because the side chains of the two residues play a completely different role in the protein. T397 is involved in the interaction with the central β-sheet, while F398 points away from the protein.

Detailed interpretation of the differences observed for different residues represents a formidable challenge. It is well-known that line shapes can be used to calculate off-rates for two-state reactions (*6*). These rates are not necessarily a simple reflection of local contacts between ligand and protein, but rather monitor the response of the protein to the ligand binding. For example, residues such as E345 or K346 that are not directly involved in contacts with the ligand experienced an induced chemical shift change associated with line broadening which reflects the rate of conversion between the fold of the complex and that of the free form. The associated lifetime τ_{off} describes the time the protein spends in the bound state. In this sense, the apparent off-rates must be understood as local dynamics induced by ligand interaction.

The conclusion that the local off-rates represent local dynamics provides a way of reconciling NMR results with

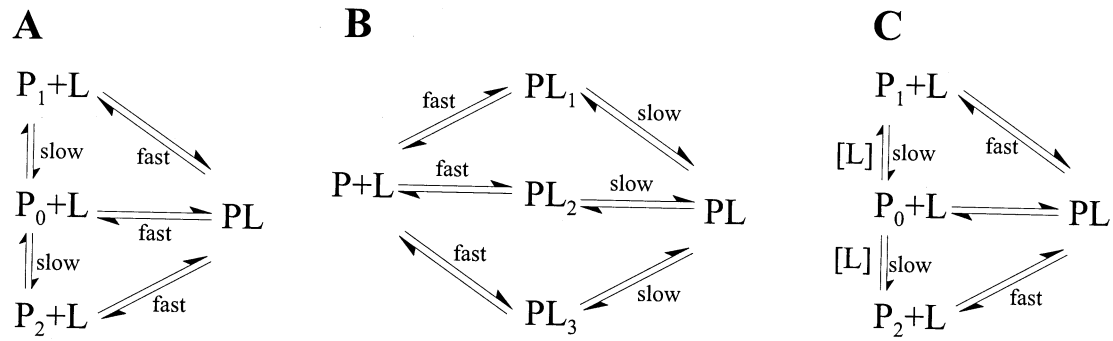

FIGURE 11: Potential mechanisms for SH2 ligand interactions.

those of surface plasmon resonance (SPR) measurements where off-rates of 1.2×10^{-3} s^{-1} (*65*) and in a more recent study even 0.6 s^{-1} (*66*) were reported. Slow rearrangements on a millisecond to second time scale as rate-determining steps for ligand binding may explain this difference because SPR measurements observe the entire process of releasing the peptide. This interpretation is possibly consistent with thermodynamic data of various SH2 constructs which suggested that a conformational change must occur during binding (*67*). Ladbury et al. assumed that conformational change must be small and limited to loop regions.

From this point of view, relatively high off-rates in the ptyr pocket (red and yellow region in αA in Figure 1A) may be interpreted as fast but low-affinity correlated processes in the ptyr pocket, whereas binding in the ptyr+3 region is characterized by lower off-rates (blue in the EF and BG loop, in βD, and in βD′). This observation sheds light on the dynamics of the binding process. Most likely, the peptide interacts rapidly with low affinity in the ptyr pocket followed by slower processes in the hydrophobic binding region which are important for high-affinity (lower off-rates).

SH2 Mutants. Each of the mutants studied here exhibited line shapes that could be readily distinguished, not only from those of the wild type but also from each other. The qualitative behavior of the line shapes of wild-type and mutant SH2s clearly showed that altered binding and specificity of mutants must be associated with different types of kinetic mechanisms.

Three different types of behavior were observed. A mutant such as I381Y shows a simple reduction in affinity as shown by higher off-rates. In this regard, it looks much like wild-type SH2 interacting with a poor ligand such as ptyr. There was little change in the qualitative nature of the titrations. Interestingly, the lowered affinity was uniform across the structure, not limited to the region of the mutation.

P427L, a mutant altered in βG near the C-terminus of the SH2, exhibited very different behavior. Here we have observed complex lines with many shoulders all over the protein. Intensities of lines were reduced during the titration. Superficially, these lines resembled line shapes for low off-rates, although the affinity measured by other methods is low. For some residues (e.g., F392), intermediate lines disappeared completely. This reflection of weak binding is quite different from the weak binding of ptyr to the wild-type SH2 or the weak binding of MT to the I381Y mutant where the intensities of the intermediate lines were hardly reduced. Clearly, weak binding in the case of P427L cannot just be ascribed to high off-rates in one-step binding reactions ($P + L \rightleftharpoons PL$, with k_{on} being the forward rate and k_{off} being the reverse rate). A more complex mechanism involving multiple conformers in intermediate spectra must be involved. One possible explanation may be that off-rates are indeed on the order of 100−1000 s^{-1} but on-rates are relatively low. For a K_D of 10^{-3} and a k_{off} of 1000 s^{-1}, the on-rate must be 10^6, 3 orders of magnitude lower than diffusion-controlled rates. Low on-rates might reflect a low availability of protein conformers suitable for ligand interaction. For example, if in Figure 11C encounter with ligand did not result in formation of suitable species for binding, then the interaction would be poor. Another slightly different interpretation might be nonproductive binding by many conformers in the ensemble. In this case, such nonproductive interactions must be reversed before subsequent interactions with conformers which are more favorable for high-affinity interactions. Such a mechanism would also reduce the apparent on-rate.

Mutation of P395 to S, resulting in lower affinity for the MT peptide, has a different kinetic basis than either the I381Y or P427L mutation. The defect in binding of the MT peptide by the P395S mutant is reflected in the appearance of kinetic intermediates with a distinct chemical shift observed for most residues that serves as a kind of "kinetic knot". In principle, this situation can be described by Figure 11C where P interacts with L to form different intermediates PL_i which convert slowly into the final product. Depending on the ratio of all the rates, intermediates PL_i will build up and the conversion between PL and PL_i will show slow exchange line shapes. This can be interpreted as a kinetic hindrance of binding. A more detailed model along with full structural analysis will be developed elsewhere (U. Günther, manuscript in preparation).

In summary, this work develops an approach to studying the mechanism of protein−ligand interactions using line shape analysis. Line shape analysis is useful to probe processes on a microsecond to millisecond time scale. The range of rates accessible for quantitative analysis is similar to the range of rates which can be analyzed by CPMG measurements. However, line shape analysis has an inherent advantage in that it gives insight into the mechanism underlying an exchange process.

The observed line shapes require that the interactions of the p85 N-SH2 with ligand involve rearrangements during the binding process. Slow kinetic processes in loops or regions adjacent to loops determine the overall rate of the protein−ligand interaction. Since slow exchange in the free SH2 was not observed, we propose a quasi-allosteric model for the interaction with the ligand. The finding that several conformers exist on the binding pathway presents a serious challenge to studies of slow chemical exchange. R_2 dispersion

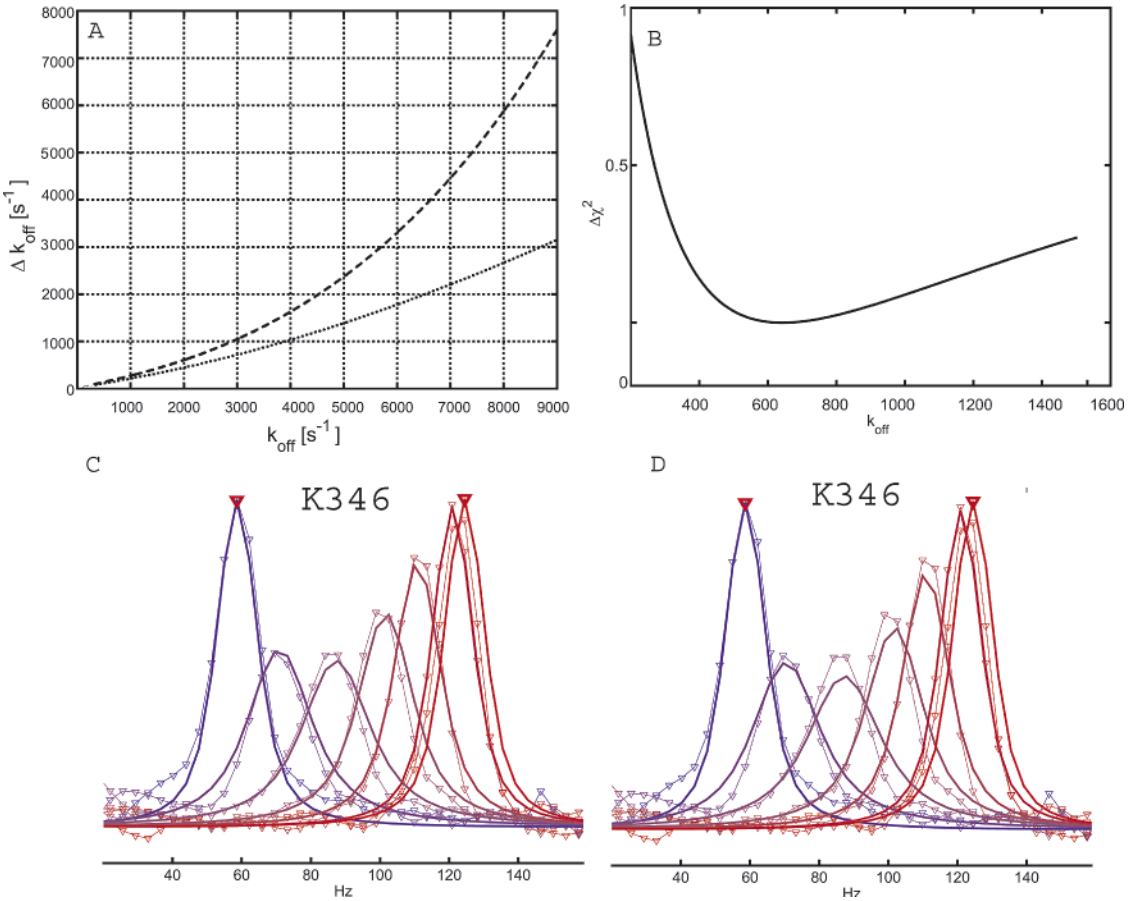

FIGURE 12: (A) Upper and lower error of Δk_{off} for theoretical line shapes simulated for a frequency separation of 150 Hz and a line width of 15 Hz (see the Appendix). (B) $\Delta\chi^2 = \chi_k^2 - \chi_{ref}^2$ [$\chi_k^2 = \sum(LS_{sim,k} - LS_{exp})^2$ and χ_{ref}^2 is the χ_k^2 for the optimal rate k_{ref}] for K346 calculated as described in the Appendix. (C) Theoretical and simulated line shapes for K346 and a k_{off} of 640 s^{-1} and (D) theoretical and simulated line shapes for K346 and a k_{off} of 550 s^{-1}.

is usually interpreted employing a two-state model. Considering the complexity of mechanisms observed for the p85 N-SH2, such a simplification would clearly not be justified. The study of line shapes in mutants showed that three different mutants with reduced binding affinity revealed completely different line shape patterns reflecting different mechanisms of binding. It will be of considerable interest to see if the complexity of the kinetic mechanism observed here for the N-SH2 is common in the interactions of other proteins with ligands.

APPENDIX

Error Estimation. The error of k_{off} cannot be determined by typically used error estimation protocols, mainly because it is very asymmetric. For high rates, i.e., fast exchange, with little line broadening, curves will be very insensitive to changes in the rate. For lower rates, small changes in rates will cause relatively large changes in line shapes. For the same reason, the upper error is usually larger than the lower error. This is illustrated in Figure 12A which shows a theoretically determined error of k_{off} to higher (dashed line) and to lower (dotted line) off-rates for values of k_{off} between 1 and 8000 s^{-1}. This error was calculated using simulated line shapes for a frequency separation of 150 Hz and an off-rate off 640 s^{-1}. Here the value of χ^2 [$=\sum(LS_{640} - LS_k)$ for k = 550 Hz (χ_{ref}^2)] was chosen as an arbitrary standard because the line shapes obtained for this value appeared to be clearly distinct (Figure 12B,C). The calculated error in k_{off} shown in Figure 12A reflects the change in k_{off} which yields the same χ^2 that was obtained for a k_{off} of 550 s^{-1}. The two curves demonstrate that the upper error increases faster than the lower error. For off-rates around 8000 s^{-1}, the relative error exceeds 100%. These error curves represent the accuracy at which *ideal* line shapes can be simulated for a given set of standard conditions.

Calculation of error estimates for experimental line shapes was based on a similar procedure. One of the underlying problems was the fact that the value of χ^2 [$=\sum(LS_{exp} - LS_{sim,k_{off}})^2$] depends strongly on artifacts in the spectra. These may include small baseline distortions outside the peak area and signals outside the simulated peaks. Such artifacts do not influence the k for which the minimal χ^2 is observed. However, these χ^2 values obtain almost arbitrary values caused by even small artifacts. They also change significantly depending on the number of experimental data points used in the simulation. For this reason, they do not provide a good error estimate. For this reason, we calculate $\Delta\chi^2 = \chi_\kappa^2 - \chi_{ref}^2$, where $\chi_\kappa^2 = \sum(LS_{sim,k} - LS_{exp})^2$ and χ_{ref}^2 is the χ^2 for the optimal rate. $\Delta\chi^2$ is very insensitive to the offset and to peaks outside the simulated signals and provides a good relative estimate for the error. As a reference, we use the χ^2 obtained for a k_{off} of 550 s^{-1} for K346. The line shapes for K346 are shown in panels B and C of Figure 12 [k_{off} = 640 s^{-1} (C) and k_{off} = 550 s^{-1} (D)]. The values for upper and lower errors are listed separately in Table 1. It is important to mention that the observed error of experimental lines was

usually very close to the error for theoretical curves without noise. The reason is that the theoretical error is large compared to the influence of noise on peaks in spectra.

ACKNOWLEDGMENT

We thank H. Rüterjans for kindly giving U.G. access to his laboratory.

REFERENCES

1. Hoyt, D., Harkins, R., Debanne, M., O'Connor-McCourt, M., and Sykes, B. (1994) *Biochemistry 33*, 15283−15292.
2. Balbach, J., Forge, V., Lau, W., Nuland, N., Brew, K., and Dobson, C. (1996) *Science 274*, 1161−1163.
3. Hensmann, M., Booker, G. W., Panayotou, G., Boyd, J., Linacre, J., Waterfield, M., and Campbell, I. D. (1994) *Protein Sci. 3*, 1020−1030.
4. Sykes, B. D., and Scott, M. D. (1972) *Annu. Rev. Biophys. Bioeng. 1*, 27−50.
5. Rao, B. (1989) *Methods Enzymol. 176*, 279−311.
6. Sudmeier, J. L., Evelhoch, J. L., and Jonsson, N. (1980) *J. Magn. Reson. 40*, 377−390.
7. Günther, U., and Schaffhausen, B. (2002) *J. Biomol. NMR 22*, 201−209.
8. Corvera, S., and Czech, M. (1998) *Trends Cell Biol. 8*, 442−446.
9. Odorizzi, G., Babst, M., and Emr, S. (2000) *Trends Biochem. Sci. 25*, 229−235.
10. Leevers, S., Vanhaesebroeck, B., and Waterfield, M. (1999) *Curr. Opin. Cell Biol. 11*, 219−225.
11. Rameh, L., and Cantley, L. (1999) *J. Biol. Chem. 274*, 8347−8350.
12. Alessi, D., and Downes, C. (1198) *Biochim. Biophys. Acta 1436*, 151−164.
13. Fruman, D., Meyers, R., and Cantley, L. (1998) *Annu. Rev. Biochem. 67*, 481−507.
14. Shepherd, P., Withers, D., and Siddle, K. (1998) *Biochem. J. 333*, 471−490.
15. Hawkins, P., Welch, H., McGregor, A., Eguinoa, A., Gobert, S., Krugmann, S., Anderson, K., Stokoe, D., and Stephens, L. (1997) *Biochem. Soc. Trans. 25*, 1147−1151.
16. Cantrell, D. (2001) *J. Cell Sci. 114*, 1439−1445.
17. Sotsios, Y., and Ward, S. (2000) *Immunol. Rev. 177*, 217−235.
18. Selheim, F., Holmsen, H., and Vassbotn, F. (2000) *Platelets 11*, 69−82.
19. Valius, M., and Kazlauskas, A. (1993) *Cell 72*, 779−790.
20. Fantl, W. J., Escobedo, J. A., Martin, G. A., Turck, C. W., del Rosario, M., McCormick, F., and Williams, L. T. (1992) *Cell 69*, 413−423.
21. Wurmser, A., Gary, J., and Emr, S. (1999) *J. Biol. Chem. 274*, 9129−9132.
22. Corvera, S., D'Arrigo, A., and Stenmark, H. (1999) *Curr. Opin. Cell Biol. 11*, 460−465.
23. Derman, M. P., Toker, A., Hartwig, J. H., Spokes, K., Falck, J. R., Chen, C. S., Cantley, L. C., and Cantley, L. G. (1997) *J. Biol. Chem. 272*, 6465−6470.
24. Wennstrom, S., Hawkins, P., Cooke, F., Hara, K., Yonezawa, K., Kasuga, M., Jackson, T., Claesson-Welsh, L., and Stephens, L. (1994) *Curr. Biol. 4*, 385−393.
25. Meili, R., Ellsworth, C., Lee, S., Reddy, T., Ma, H., and Firtel, R. (1999) *EMBO J. 18*, 2092−2105.
26. Nolan, R. D., and Lapetina, E. G. (1990) *J. Biol. Chem. 265*, 2441−2445.
27. Kucera, G., and Rittenhouse, S. (1990) *J. Biol. Chem. 265*, 5345−5348.
28. Traynor-Kaplan, A. E., Thompson, B. L., Harris, A. L., Taylor, P., Omann, G. M., and Sklar, L. A. (1989) *J. Biol. Chem. 264*, 15668−15673.
29. Ninomiya, N., Hazeki, K., Fukui, Y., Seya, T., Okada, T., Hazeki, O., and Ui, M. (1994) *J. Biol. Chem. 269*, 22732−22737.
30. Kaplan, D., Whitman, M., Schaffhausen, B., Raptis, L., Garcea, R., Pallas, D., Roberts, T., and Cantley, L. (1986) *Proc. Natl. Acad. Sci. U.S.A. 83*, 3624−3628.
31. Chang, H., Aoki, M., Fruman, D., Auger, K., Bellacosa, A., Tsichlis, P., Cantley, L., Roberts, T., and Vogt, P. (1997) *Science 276*, 1848−1850.
32. Aoki, M., Batista, O., Bellacosa, A., Tsichlis, P., and Vogt, P. (1998) *Proc. Natl. Acad. Sci. U.S.A. 95*, 14950−14955.
33. Freund, R., Dawe, C. J., Carroll, J. P., and Benjamin, T. L. (1992) *Am. J. Pathol. 141*, 1409−1425.
34. Minshall, C., Arkins, S., Freund, G., and Kelley, K. (1996) *J. Immunol. 156*, 939−947.
35. Yao, R., and Cooper, G. M. (1995) *Science 267*, 2003−2006.
36. Shaw, L., Rabinovitz, I., Wang, H., Toker, A., and Mercurio, A. (1997) *Cell 92*, 949−960.
37. Klippel, A., Escobedo, J. A., Fantl, W. J., and Williams, L. T. (1992) *Mol. Cell. Biol. 12*, 1451−1459.
38. McGlade, C., Ellis, C., Reedijk, M., Anderson, D., Mbamalu, G., Reith, A., Panayotou, G., End, P., Bernstein, A., Kazlauskas, A., Waterfield, M., and Pawson, T. (1992) *Mol. Cell. Biol. 12*, 991−997.
39. Hu, P., Margolis, B., Skolnik, E. Y., Lammers, R., Ullrich, A., and Schlessinger, J. (1992) *Mol. Cell. Biol. 12*, 981−990.
40. Yoakim, M., Hou, W., Liu, Y., Carpenter, C. L., Kapeller, R., and Schaffhausen, B. S. (1992) *J. Virol. 66*, 5485−5491.
41. Marengere, L. E., and Pawson, T. (1994) *J. Cell Sci., Suppl. 18*, 97−104.
42. Cohen, G., Ren, R., and Baltimore, D. (1995) *Cell 80*, 237−248.
43. Schaffhausen, B. (1995) *Biochim. Biophys. Acta 1242*, 61−81.
44. Schlessinger, J. (1994) *Curr. Opin. Genet. Dev. 4*, 25−30.
45. Kuriyan, J., and Cowburn, D. (1997) *Annu. Rev. Biophys. Biomol. Struct. 26*, 259−288.
46. Booker, G. W., Breeze, A. L., Downing, A. K., Panayotou, G., Gout, I., Waterfield, M. D., and Campbell, I. D. (1992) *Nature 358*, 684−687.
47. Nolte, R. T., Eck, M. J., Schlessinger, J., Shoelson, S. E., and Harrison, S. C. (1996) *Nat. Struct. Biol. 3*, 364−374.
48. Breeze, A., Kara, B., Barratt, D., Anderson, M., Smith, J., Luke, R., Best, J., and Cartlidge, S. (1996) *EMBO J. 15*, 3579−3589.
49. Siegal, G., Davis, B., Kristensen, S., Sankar, A., Linacre, J., Stein, R., Panayotou, G., Waterfield, M., and Driscoll, P. (1998) *J. Mol. Biol. 276*, 461−478.
50. Weber, T., Schaffhausen, B., Liu, Y., and Günther, U. (2000) *Biochemistry 39*, 15860−15869.
51. Songyang, Z., Shoelson, S., Chaudhuri, M., Gish, G., Pawson, T., Haser, W., King, F., Roberts, T., and Ratnofsky, S. (1993) *Cell 72*, 767−778.
52. Songyang, Z., Gish, G., Mbamalu, G., Pawson, T., and Cantley, L. (1995) *J. Biol. Chem. 270*, 26029−26032.
53. Millet, O., Loria, J. P., Kroenke, C. D., Pons, M., and Palmer, A. G., III (2000) *J. Am. Chem. Soc. 122*, 2867−2877.
54. Loria, J., Rance, M., and Palmer, A. I. (1999) *J. Biomol. NMR 15*, 151−155.
55. Günther, U., Liu, Y., Sanford, D., Bachovchin, W., and Schaffhausen, B. (1996) *Biochemistry 35*, 15570−15581.
56. Yoakim, M., Hou, W., Songyang, Z., Liu, Y., Cantley, L., and Schaffhausen, B. (1994) *Mol. Cell. Biol. 14*, 5929−5938.
57. Mullane, K., Ratnofsky, M., Culleré, X., and Schaffhausen, B. (1998) *Mol. Cell. Biol. 18*, 7556−7564.
58. Zhang, Z., Maclean, D., Thieme-Sefler, A., Roeske, R., and Dixon, J. (1993) *Anal. Biochem. 211*, 7−15.
59. Zhao, Z., Zander, N., Malencik, D., Anderson, S., and Fischer, E. (1992) *Anal. Biochem. 202*, 361−366.
60. Günther, U., Ludwig, C., and Rüterjans, H. (2000) *J. Magn. Reson. 145*, 101−108.
61. Shoelson, S. E., Sivaraja, M., Williams, K. P., Hu, P., Schlessinger, J., and Weiss, M. A. (1993) *EMBO J. 12*, 795−802.
62. French, T., and Hammes, G. (1965) *J. Am. Chem. Soc. 87*, 4669−4673.
63. Markley, J., and Jardetzky, O. (1970) *J. Mol. Biol. 50*, 223−233.
64. Volkman, B., Lipson, D., Wemmer, D., and Kern, D. (2001) *Science 291*, 2429−2433.
65. Payne, G., Shoelson, S. E., Gish, G. D., Pawson, T., and Walsh, C. T. (1993) *Proc. Natl. Acad. Sci. U.S.A. 90*, 4902−4906.
66. de Mol, N., Plomp, E., Fischer, M., and Ruijtenbeek, R. (2000) *Anal. Biochem. 279*, 61−70.
67. O'Brien, R., Rugman, P., Renzoni, D., Layton, M., Handa, R., Hilyard, K., Waterfield, M., Driscoll, P., and Ladbury, J. (2000) *Protein Sci. 9*, 570−579.
68. Eck, M. J., Shoelson, S. E., and Harrison, S. C. (1993) *Nature 362*, 87−91.

BI0202528